NANOFUNCTION

Beyond CMOS Nanodevices for Adding Functionalities to CMOS

Network of Excellence

WP 2: Exploration of new materials, devices and technologies for Energy Harvesting

Task 2.3 : New materials and device architecture for nanostructured solar cells

Deliverable "D2.2: Nanowire-based photovoltaic solar cells : experiments and simulations"

Main Author(s): A. Kaminski-Cachopo, M. Zanuccoli, T. Baron

Dissemination level: Public

Due date of deliverable: M25

Actual submission date: M25

Project funded by the European Commission under grant agreement n°257375

LIST OF CONTRIBUTORS

Partner	Acronym	Laboratory Name	Name of the contact
Institut Polytechnique de Grenoble	Grenoble INP	FMNT/IMEP-LAHC	A.Kaminski-Cachopo
Institut Polytechnique de Grenoble	Grenoble INP	FMNT/IMEP-LAHC	M. Mouis
Institut Polytechnique de Grenoble	Grenoble INP	FMNT/IMEP-LAHC	F. Ducroquet
Institut Polytechnique de Grenoble	Grenoble INP	FMNT/IMEP-LAHC	J. Michallon
Institut Polytechnique de Grenoble	Grenoble INP	FMNT/IMEP-LAHC	M. Daanoune
Institut Polytechnique de Grenoble	Grenoble INP	FMNT/IMEP-LAHC	I.Ionica
Institut Polytechnique de Grenoble	Grenoble INP	FMNT/LTM	T. Baron
Institut Polytechnique de Grenoble	Grenoble INP	FMNT/LTM	B.Salem
IUNET-University of Bologna, Via Venezia 260, 47521 Cesena (FC), Italy	IUNET		C.Fiegna
IUNET-University of Bologna, Via Venezia 260, 47521 Cesena (FC), Italy	IUNET		M. Zanuccoli

TABLE OF CONTENTS

Deliverable Summary

Silicon nanowires based solar cells are an attractive approach to realise solar cells with efficient light trapping scheme and high collection efficiency in case of radial junctions. In fact, the high-aspect-ratio of nanowires permits to reduce significantly solar cell thickness without loss of optical absorption while simultaneously providing effective carrier collection in the case of radial junction. This structure benefits from the long optical path within the wire length and by exploiting a radial junction, a shorter path for carrier collection corresponding to the wire radius is achieved, leading to a smaller carrier recombination rate. Efficiencies similar or higher to the ones obtained with first generation solar cells (about 14-18%) are expected for single junction nanowire solar cells with a cost reduction thanks to material consumption and to low cost growth methods.

This activity driven by IUNET and FMNT was devoted to the simulation, elaboration and characterization of nanowires and nanowires based solar cells in order to define an optimized photovoltaic structure from an optical and electrical point of view. Two types of materials have been analysed : silicon nanowires as the reference material with indirect band gap ; ZnO nanowires with CdTe radial heterojunction as the direct band gap material for comparison.

Concerning the Si nanowires synthesis, the activity was focused on Vapor Liquid Solid method which has the advantage of being a bottom-up and low cost technology. Gold was used as catalyst for Si nanowires growth and special attention was given to nanowires doping using gas mixture including HCl to keep the same surface state as undoped nanowires. The synthesis of ZnO/CdTe core/shell NW arrays has been performed by using chemical and physical growth methods such as Chemical bath deposition CBD and close space sublimation CSS.

Simulations activities were performed using a RCWA software for the optical simulations and a commercial TCAD tool for electrical simulations. During this task, an important work has been performed to develop and verify the validity of the simulator and of the models used for the nanowires simulation. Solar cells based on Si and ZnO/CdTe nanowires have been simulated and an optimized geometry from an optical point of view has been defined for each type of material. It has been shown that the nanowire structure permits to increase significantly photons absorption compared to planar structure with the same amount of material especially in the case of indirect band gap semiconductor. Electrical simulations have been shown that interfacial recombination play an important role on the efficiency of the solar cell and special care should be given to interfacial passivation.

Finally, optical and electrical simulations have been performed on nanowires array and nanowires based solar cells. Reflectivity and transmittance measurements have been realized with an integrating sphere on ZnO/CdTe structure showing a strong absorption as indicated by the simulations. Reflectivity measurements on silicon nanowires and silicon nanowire based solar cells have shown also an improvement of the light trapping due to the surface structuration. Electrical characterization performed on c-Si (crystalline silicon) nanowires array and on a-Si (amorphous silicon)/c-Si heterojunction solar cells have confirmed the strong influence of surface and interface recombination.

1. First activity : Nanowires synthesis and physical characterisation

1.1 Introduction

Nanowires (NW) based solar cells are good candidates to decrease the cost of photovoltaic energy due to the increase of light absorption and carrier collection efficiency. There are two main approaches to elaborate the nanowires arrays: a bottom-up approach based on the growth of the nanowires usually by CVD (Chemical Vapor deposition) and a top-down approach based on etching methods. For photovoltaic energy production, it is preferable to use low cost and competitive technologies. Therefore bottom-up techniques are preferable to top-down methods that consume material and increase the cost of the device. In this study we have focus on bottom-up low cost technologies to grow nanowires arrays instead of more expensive etching techniques.

Si NW arrays for photovoltaic applications are usually grown by CVD on top of silicon wafer, glass substrate or metal [1-5]. The most used technique is the vapor liquid solid (VLS) method which uses a metal catalyst to form a liquid eutectic with the desired nanowire material. Junction is preferably radial than axial for photovoltaic applications in order to increase collection probability (minority carriers only have to travel on a maximum distance corresponding to the radius of the nanowire). pn junction can be realized by doping but due to the small diameter of the nanowire, there might be a complete doping of the nanowire instead of just the surface. Another way is to deposit a conformal and doped polysilicon layer on the nanowire. However the interface is usually highly recombinant. In order to passivate the surface of the nanowire and to create a junction, an interesting structure is the amorphous silicon / crystalline silicon (a-Si/c-Si) heterostructure which has already demonstrated high efficiencies for first generation solar cells [6]. This structure will be analysed in the second and third activity of this deliverable, this first activity being essentially devoted to the Si nanowires growth and doping.

Increasing efforts have also been dedicated to the development of nanostructures based on ZnO thanks to its ability to grow within the NW morphology by a wide variety of growth methods such as CVD [7], chemical bath deposition (CBD) [8] or electro-deposition [9]. Such NWs can be covered with CdSe [10], ZnS [11], ZnSe [12], or CdTe [8,13] in order to create a type II band alignment heterojunction. The latter is a very efficient absorbing material with a bandgap energy of 1.5 eV at room temperature and will be also studied in this work in order to perform a comparison with Si nanowires which are less absorbent due to Si indirect band gap.

Relatively low experimental efficiencies obtained up to now (experimental power conversion efficiency of 7.9% has already been reported for grown Si NW arrays [14]) are mainly due to high surface recombination velocity and series and shunt resistance. There are still technological improvements needed to grow high quality nanowires and to reduce surface recombination.

The objective of this task is to develop a low cost efficient process to grow nanowires arrays based on silicon and ZnO. Si nanowires doping was optimized to obtain high quality doped nanowires for photovoltaic applications.

1.2. Methodology / Networking and collaboration

SiNWs were grown by FMNT in a low-pressure CVD reactor operating at 600 or 650 °C and 3 Torr total pressure with Au as catalysts. Hydrogen (H_2) was used as the carrier gas, while silane SiH_4 was used as the Si precursor. p-type and n-type doping were achieved by introducing B_2H_6 and PH_3 respectively into the reactor, with P_{B2H6}/P_{SiH4} and P_{PH3}/P_{SiH4} ratios in the 10^{-6}–10^{-2} range. Depending on the experiment, an additional HCl flux could be introduced into the reactor.

As it is a crucial point for photovoltaic application to control the formation of a PN junction, we have focused our attention on the doping of Si NWs. We have examined the effect of the HCl introduction in the growth recipes used for making doped SiNWs. In particular, we show that p- and n-type doped SiNWs can be obtained using $HCl/SiH_4/B_2H_6$ and $HCl/SiH_4/PH_3$ gas mixtures respectively while retaining the same surface state—tapering, roughness and presence of gold clusters—as the undoped SiNWs grown using the HCl/SiH_4 gas mixture. It is a very good point for further core shell NWs growth. It is, in particular, shown that efficient p-type doping of SiNWs can be achieved with the same ease as for n-type ones and without an amorphous shell growth.

The synthesis of ZnO/CdTe core/shell NW arrays has been performed by FMNT on fluorine-doped tin oxide FTO thin films by using low-cost chemical and physical growth methods such as CBD and close space sublimation CSS.

1.3. Results and discussion / Perspectives

Figure 1 presents p-type SiNWs grown with SiH_4 and B_2H_6 (without HCl) on a dewetted gold thin film at 650 °C for different dopant to silane ratios. We observe an increase of the tapering and the surface roughness with the increase of P_{B2H6}/P_{SiH4} ratio.

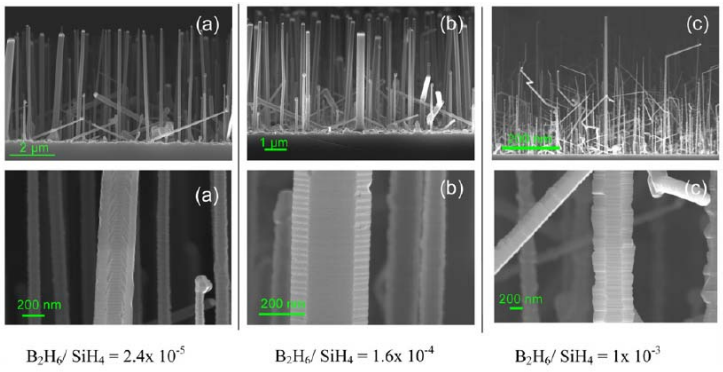

Figure 1 : SEM images of p-doped SiNW growth with different P_{B2H6}/P_{SiH4} ratios, at 650 °C, 1.5 Torr total pressure, without HCl. The faceting increases with the B/Si ratio due to 2D growth. The tapering increases with P_{B2H6}/P_{SiH4} ratio

Figure 2 compares the growth of p-type and n-type SiNWs with and without HCl. The wires were grown at 650 °C, 3 Torr and $P_{B2H6}/P_{SiH4} = 1x10^{-3}$ using 100 nm diameter gold colloids. HCl-free recipes lead to very different growth regimes compared with the chlorinated counterparts. Without HCl, the strong catalyst migration (see the inset in figure 2(c)) during growth can induce a total depletion of the catalytic head long before the end of the deposition step. The corresponding wires are much shorter in height and not terminated by a catalyst. In addition, significant tapering and a rough surface are clearly

observed. The addition of HCl in the B_2H_6 and SiH_4 mixture leads to a considerable increase of the growth yield per colloid, a great reduction of wire tapering, despite the quite long 20 µm length of the NWs.

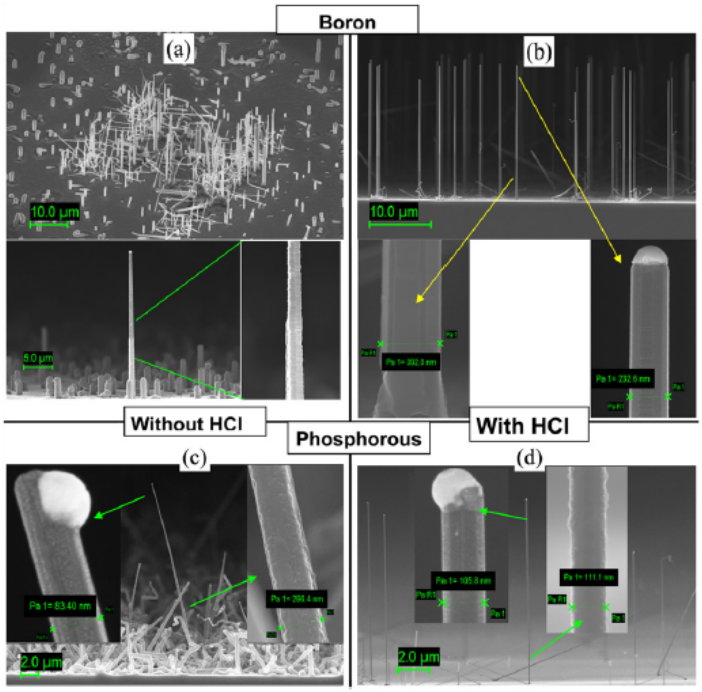

Figure 2 : SEM images of p-doped ((a), (b)) and n-doped ((c), (d)) SiNWs, grown from gold colloids (100 nm diameter) with dopant to silane ratio equal to 10^{-3} in both cases, at 650 °C for the boron doping and 600 °C for the phosphorous doping, without HCl ((a), (c)) and with HCl ((b), (d)).

In figure 3 we present the apparent resistivity as a function of the dopant gas to silane ratio for the n- and p-doped SiNWs. These results are obtained on wires typically 20–30 µm in length, 100–200 nm in diameter, and display the mean value for the apparent resistivity, when measured in several places across the wire. The values show a decrease of the resistivity as the dopant gas to silane ratio increases. The smallest mean apparent resistivity measured from the HCl wires was found to be 6mΩ.cm for p-type wires, corresponding to $N_A = 10^{19}$ cm^{-3}, based on use of the bulk mobility. The corresponding value for n-type wires was measured at 0,6 mΩ cm ($N_D = 10^{20}$ cm^{-3}).

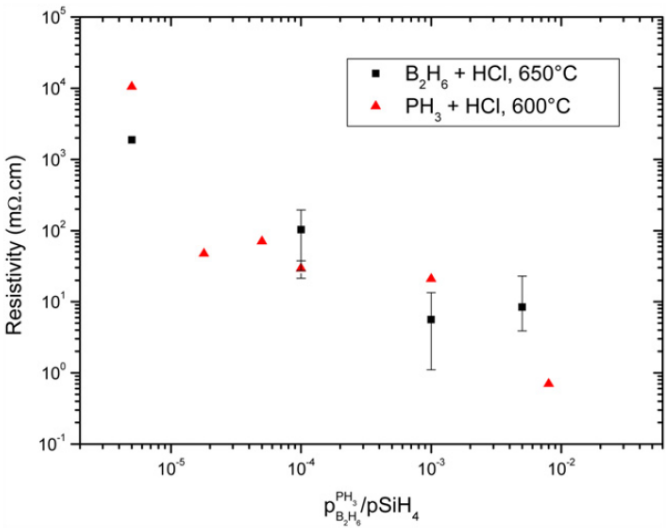

Figure 3 : Mean apparent resistivity of SiNWs grown with HCl for phosphorous doping at 600°C and boron doping at 650 °C.

2. Second activity : Optical and electrical simulation of nanowires based solar cells

2.1 Introduction

Nanowires solar cells are expected to outperform the thin-film counterpart in terms of optical absorbance, however the geometry of the array has to be optimized in order to maximize the carrier absorption for a given configuration of the media. Optimization of regular arrays involves the proper sizing of the heights, of the diameters as well as of the wire periodicity. As the dimensions of the investigated structures are on the same order of magnitude of the incident radiation wavelength, the optical properties of nanowires are influenced by diffraction effect. Interference and multiple reflection effects are also responsible of the absorption enhancement. Therefore the optical simulations of nanostructures must be performed by means of rigorous solvers of Maxwell equations like the Finite Element Method (FEM) [15], the Transfer Matrix Method (TMM) [16] and the Finite Difference Time Domain (FDTD) [17]. Methods like FEM and FDTD are remarkably cpu- and memory-demanding especially for applications involving the optical simulations of nano- and micro-structured solar cells. Recently the Rigorous Coupled-Wave Analysis (RCWA) method [18] based on the modal expansion of the electromagnetic field has been adopted for the numerical simulation of the light propagation in thin-film solar cells [19]. In RCWA the approximation is introduced by the number of Fourier expansion modes included in the calculation. However, RCWA allows to attain a good trade-off between accuracy and computational resources requirement, especially if compared with FDTD method [20].

In [21] the InP nanowires with dimensions in the range of those of the structure investigated in this work have been simulated by means of a RCWA simulator in order to study the impact of the geometry on the absorbance properties. In [22] an amorphous silicon (a-Si) nanowire has been theoretically investigated by means of a commercial optical simulator and by a 2-D TCAD simulator [23]. A

conversion efficiency of 11.6% and a photocurrent enhancement of about 40% have been reported with reference to the thin-film planar counterpart for a 4000nm-thick wire. In [24] the authors use the TMM to calculate the optical absorbance of vertically-aligned silicon nanowire (SiNW) arrays, reporting for an optimized structure (periodicity 600nm, wire diameter 540nm, height 2330nm) an enhancement of ultimate conversion efficiency above 70% with respect to the planar configuration. The spatially resolved optical generation map has been calculated by MEEP [25]. In [26] a theoretical analysis and modelling of light trapping in GaAs nanowire arrays (NWAs) has been performed by a 3-D FDTD simulator and the electric simulation by a commercial TCAD tool [23], the optimized NWA has been reported to exhibit a conversion efficiency of 22.3%. Kelzenberg and authors in [27] use 3-D FDTD simulations in order to calculate the optical absorbance and the generation rate map of silicon wire arrays and incorporate the spatially resolved optical generation map in a 2-D TCAD [23] simulation performed by exploiting the cylindrical symmetry of the wire. Simulations have been carried out by considering a wavelength resolution of approximately 50nm in order to limit the number of monochromatic optical simulations. Partial spectral averaging has been adopted to suppress coherence artefacts in the simulation results.

In this work, in order to investigate from a theoretical point of view three different topologies of the nanowire array solar cells depicted in Figure 5 (c-Si/AZO/glass, a-Si/c-Si/AZO/Glass core-shell, CdTe/ZnO/Glass core-shell), coupled electro-optical simulations have been performed. The absorbance has been maximized by optimizing the geometry of the array. The electrical performance of the optimized nanowire array in case of the a-Si/c-Si/AZO/Glass and of CdTe/ZnO/Glass core-shell devices have been investigated reporting the main figures of merit (short-circuit current density, open-circuit voltage, fill-factor and conversion efficiency) as well as the collection efficiency of the photo-generated carriers, with the aim to study the impact of the recombination mechanisms (at bulk and at surface level) on the conversion efficiency. As a matter of fact, one well-known drawback of nanowires based solar cells is the potentially high-defective larger surface area with respect to the planar device, therefore a careful modelling of recombination losses have to be performed.

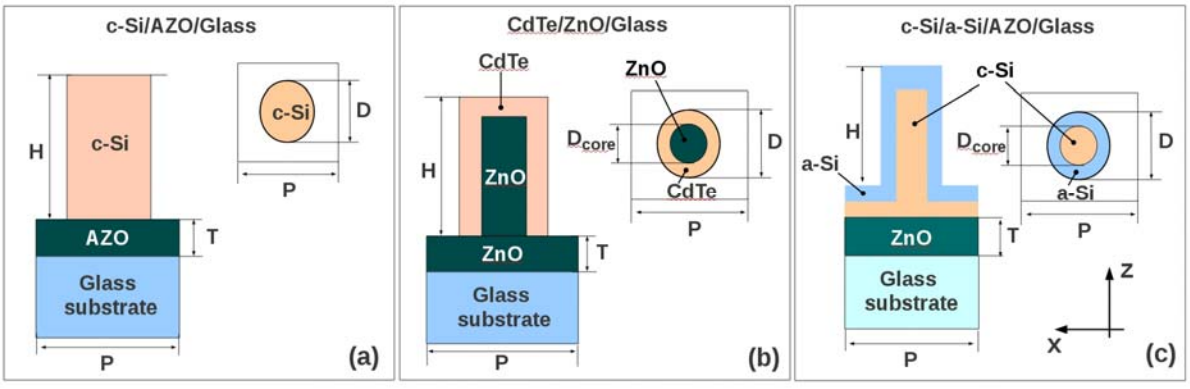

Figure 5 Cross sections of the investigated nanowires: (a) c-Si/AZO/Glass, (b) CdTe/ZnO/Glass core-shell and (c) a-Si/c-Si/AZO/Glass core-shell. Only one period of the structure is depicted. P, D and H denote the periodicity, the external diameter and the height of the wires, respectively. T is thickness of the ZnO layer.

2.2. Methodology / Networking and collaboration

Optical simulations have been performed by means of a three-dimensional (3-D) RCWA. RCWA simulator has been validated by means of a comparison with literature data and with other simulators like AFMM [28,29] (the Fourier Modal Method tool developed at Minatec, Grenoble) and the commercial FDTD tool for electromagnetic simulation (Lumerical FDTD Solution 7.5 [30]).

Figure 6a shows the comparison of the absorbance (ratio of absorbed to incident photons) calculated by RCWA with those from literature (calculated by FEM) and calculated by FDTD for an array of cylindrical silicon nanowires featuring diameter of 50nm, periodicity 100nm and heights 1160nm and 4660nm. A good agreement has been obtained.

Figure 6b shows the comparison between absorbance calculated by FDTD and RCWA of a silicon nanowire array on doped ZnO/Glass substrate (diameter 315nm, periodicity 350nm, height 1000nm) calculated by RCWA (24 Fourier modes). For FDTD a crucial numerical parameter which strongly affects accuracy is the numerical grid size. An acceptable grid size is below 4nm which leads to simulation times significantly longer than that required by RCWA. In Figure 6b the adopted grid size is 4nm.

Optical simulations have been carried out by solving the Maxwell equations in a 3-D spatial domain with the aim to investigate the impact of the geometrical parameters (periodicity, diameter, height) on the optical absorbance. The periodicity *P* is varied within the range 250nm-700nm by adopting a step of 50nm. The ratio diameter to periodicity *D/P* is varied from 0.3 up to 1.0 with a step of 0.1. *H* denotes the height of the nanowire. The simulated nanowire arrays are sketched in Fig. 6. In Fig. 6a the silicon on doped-ZnO (c-Si/AZO/Glass) is shown. Only H=1000nm has been assumed for this structure. In Figure 6b the cross section of the CdTe/ZnO/Glass core-shell nanowire is depicted. The thickness of the CdTe shell is 40nm. The optical band-gap of CdTe is 1.50 eV at room temperature (cut-off wavelength 830nm). In Figure 6c the a-Si/c-Si/ZnO/Glass core-shell is shown. The thickness of the a-Si layer is 50nm (25nm intrinsic a-Si buffer layer, 25nm of n-doped layer). The optical band-gap Eg_o of the a-Si is 1.72eV (cut-off wavelength 730nm). For all considered nanowires arrays the thickness of doped-ZnO layer is 300nm and the substrate is glass. Simulations have been performed within the range of wavelength 300nm-1200nm with a step of 10nm (5nm for the c-Si/AZO/Glass and the a-Si/c-Si/AZO/Glass core-shell) by adopting 24 Fourier modes for each axis perpendicular to the propagation direction *z*, with the exception of the a-Si/c-Si/AZO/Glass core-shell structure, for which 28 modes have been adopted only within the range 730nm-1000nm in order to enhance the accuracy in such portion of the spectrum in which the investigated structure exhibits narrow peaks and several fluctuations. Incident radiation has been considered collinear with the revolution axis of nanowire. In case of FDTD simulations, side periodic boundary conditions are applied in order to reduce the simulation domain to only one period of the array. Absorbing boundary conditions are applied along the propagation direction. In case of RCWA, since the method relies on Fourier series expansion, the structure considered is automatically periodized, thus no boundary conditions have been set. The simulated structures exhibit cylindrical symmetry therefore the simulations time as well as the required memory can be significantly reduced by exploiting symmetry with respect of *xz*- and *yz*-planes.

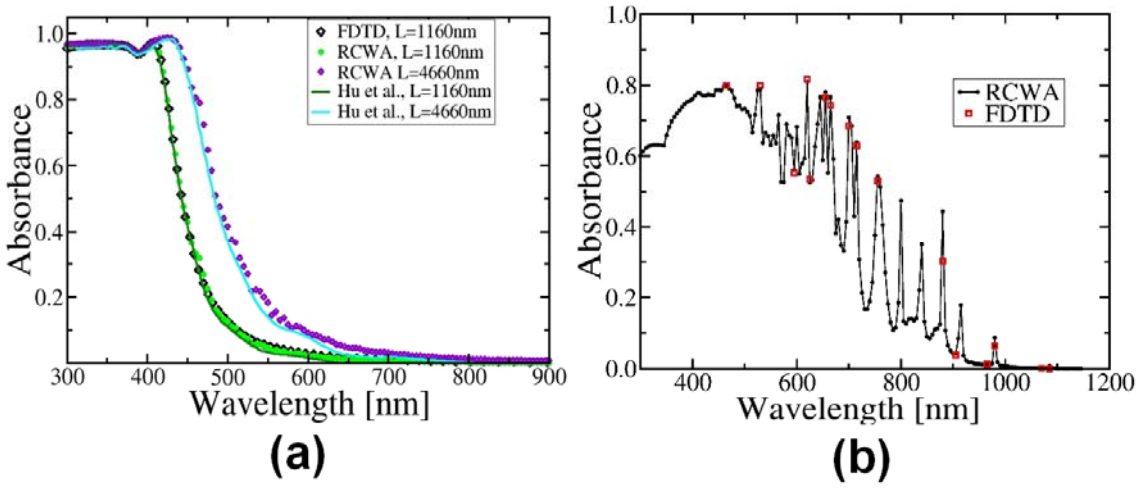

Figure 6 (a) Comparison of absorbance of a silicon nanowire array (periodicity 100nm, diameter 50nm, height 1160nm and 4460nm) calculated by RCWA, AFMM, FDTD and by FEM (Lin et al. [24]). (b) Comparison of absorbance of a silicon nanowire array on doped ZnO/Glass substrate (diameter 315nm, periodicity 350nm, height 1000nm) calculated by RCWA and by FDTD. FDTD calculations have been performed by adopting a grid size of 4nm. For RCWA the number of Fourier modes for each axis perpendicular to the propagation direction is 24.

In order to compare the simulated structures, the photo-generated current density J_{ph} has been calculated as:

$$J_{ph} = q \int_{300nm}^{1200nm} \phi_{inc}(\lambda) A(\lambda) d\lambda \quad (1)$$

where $\phi_{\mathrm{inc}}(\lambda)$ is the incident photon flux (standard ASTM G173-03 [31] Reference Spectra Global featuring Total Spectral Irradiance 1000W/m^2) at the given wavelength λ; such current density represents also the upper bound limit of the short circuit current density that can be obtained under ideal conditions (absence of recombination mechanisms) ; A(λ) is the absorptance calculated by optical simulation and q the electron charge. The calculated 3-D spatially and wavelength resolved optical generation rate $G_{opt}^{3-D}(x', y', z', \lambda) = G_{opt}^{3-D}(r \cdot \cos\varphi, r \cdot \sin\varphi, z', \lambda)$ maps are flattened to 2-D cylindrical coordinates $(r, z) = (r, z')$ by numerical interpolation and integration:

$$G_{opt}^{2-D}(x, z, \lambda) = \frac{1}{2\pi r} \int_0^{2\pi} r G_{opt}^{3-D}(r, \varphi, z, \lambda) d\varphi \quad (2)$$

Where $r = \sqrt{(x')^2 + (y')^2}$ is the radial distance and $x = r$ in the 2-D grid $(\varphi = 0)$. Electric simulation is performed by means of the state-of-the-art drift-diffusion semiconductor numerical modelling tool Sentaurus TCAD by Synopsys [23] under the assumptions of cylindrical symmetry and slight dependence of the optical generation rate profiles on the polar coordinate φ. The flattening procedure conserves the total amount of photo-generated carried inside the absorbing media. In case of the a-

Si/c-Si/AZO/Glass core-shell structure (Figure 5c), the doping concentration of the spatially uniform doping profiles are $10^{19}cm^{-3}$ and $10^{17}cm^{-3}$ for the n-doped 25nm-thick a-Si shell region and the p-doped c-Si core region, respectively. The 25nm-thick interfacial layer (between the outer p-doped shell and the c-Si core) is made of intrinsic a-Si. The top contact is modelled by the ideal ohmic contact at the cylinder and at the base interfaces. The bottom contact is modelled by the ideal ohmic contact at the c-Si/ZnO interface. Minority carrier recombination velocity at top and bottom electrodes is set to 10^7cm/s [27] Defects in a-Si regions are modelled by taking into account a continuous distribution of density of states in energy according to [22] in which the traps distribution model has been calibrated by experiments. In particular, exponential band- tails and mid-gap Gaussian distributed defects are accounted for. Recombination through deep defects in c-Si core is accounted by means of the single-trap level Shockley-Read-Hall (SRH) model. Doping dependent lifetimes are assumed according to Glunz's parameterization [32]. Carrier mobility in a-Si is set to $1cm^2/(Vs)$ and to $10cm^2/(Vs)$ for electron and hole, respectively. Mobility bad-gap for a-Si is 1.72eV; in case of the c-Si the band-gap narrowing (BGN) model by Schenk is accounted for the effective intrinsic carrier density [33]. In addition the Auger recombination model with the parameterization adopted by Altermatt in [34] and the mobility model proposed by Klaassen [35] are adopted.

The photo-generated carrier collection efficiency characteristic is calculated at approximately 30nm intervals throughout the spectral range 300nm-1200nm. The I-V characteristics are calculated by weighting the monochrome optical generation maps by the standard spectrum ASTM G173-03 [31] with irradiance $1000W/m^2$. The monochrome optical generation maps are calculated at 5nm interval in order to account for fluctuations of the absorbance characteristic within the portion of interest of the spectrum in case of the a-Si/c-Si/AZO/Glass core-shell and of the c-Si/AZO/Glass nanowire arrays, while for the CdTe/ZnO/Glass structure a 10nm-interval of wavelength is adopted.

2.3. Results and discussion / Perspectives

Figures 7a and Fig. 7b report the photo-generated current density maps calculated for the c-Si/AZO/Glass and the a-Si/c-Si/AZO/Glass core-shell nanowire arrays for H=1000nm, respectively. It is worth noting that narrow peaks around the optimum position are observed for both calculated maps. In case of the c-Si/AZO/Glass the calculated optimum configuration is that for P=350nm and D/P=0.9, leading to $J_{ph}=16.9mA/cm^2$. In case of the a-Si/c-Si/AZO/Glass core-shell the optimum periodicity *P* and *D/P* for *H*=1000nm are 500nm and 0.8, respectively, leading to $J_{ph}=18.73mA/cm^2$.

In Figure 8 the photo-generated current density maps calculated for the CdTe/ZnO/Glass core-shell nanowires with heights 1, 3 10 and 30μm are reported. A plateau of the photo-generated current density J_{ph} is observed around the optimum position. The optimum geometrical configuration (periodicity, diameter) is strongly dependent on the height as shown in Tab. 1; for periodicity *P* within the range 350nm-600nm and *D/P*=0.3-0.6, the calculated J_{ph} is within the range $23.98mA/cm^2$-$29.11mA/cm^2$. As expected the highest Jph, which increases with increasing *H*, has been obtained for *H*=30μm, however it is worth noting that the maximum theoretically obtainable J_{ph} saturates remarkably for wires thicker than 10μm. Interestingly the optimal diameter of the NW have been found to be about 200nm for the structures studied suggesting that internal multiple reflection are maximized for this particular values of CdTe thickness and ZnO diameter.

It is worth noting that (Tab. 1) the theoretically predicted photo-current density enhancement is remarkable for the c-Si/AZO/Glass array (+115%) and for the a-Si/c-Si/AZO/Glass core-shell array (+128%), with respect to the planar counterpart exhibiting the same amount of absorbing material, as shown in Figure 8. This is due to the fact that silicon is an indirect band gap material that poorly absorbs light. The optimal structure enhances the absorption because it exhibits many resonances of light within the array as it can be seen on figure 6(b) making this structure promising in term of performance. In the case of ZnO/CdTe NW arrays, since CdTe is a very good absorbing material the enhancement due to the resonances is reduced and exhibits an improvement of the short circuit current density of 40% to 70% depending on the NW height.

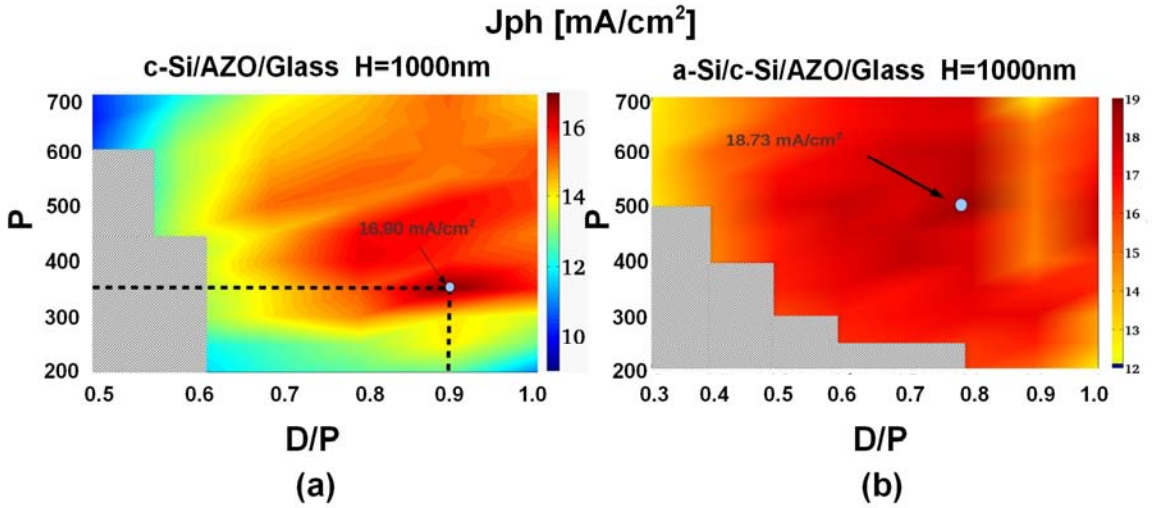

Figure 7 Photo-generated current density maps for (a) c-Si/AZO/Glass nanowires array and for (b) a-Si/c-Si/AZO/Glass core-shell featuring height H=1000nm. In the former case the optimum geometrical configuration (P=350nm, D/P=0.9) leads to J_{ph}=16.90

	Optimum Geometry				Equivalent Planar Slab			
Array Type	**H**	**P**	**D**	**D/P**	**Jph**	**Thickness**	**Jph**	**Jph Enhanc.**
	[μm]	**[nm]**	**[nm]**		**[mAcm^{-2}]**	**[nm]**	**[mAcm^{-2}]**	**[%]**
c-Si/AZO/Glass	1.0	350	315	0.9	16.90	636	7.87	+115
CdTe/ZnO/Glass	1.0	350	210	0.6	23.98	179	13.82	+70
CdTe/ZnO/Glass	3.0	400	200	0.5	27.50	380	18.16	+50
CdTe/ZnO/Glass	10	500	200	0.4	28.79	806	20.38	+40
CdTe/ZnO/Glass	30	600	180	0.3	29.11	1384	20.99	+40
a-Si/c-Si/AZO/Glass	1.0	500	400	0.8	18.73	259 (a-Si) 318 (c-Si)	8.20	+128

Tab. 1 Summary of the main results in terms of photocurrent density calculated by means of 3D optical simulations for the different topology of nanowires array. The enhancement of photocurrent density with respect to the planar counterpart is also reported.

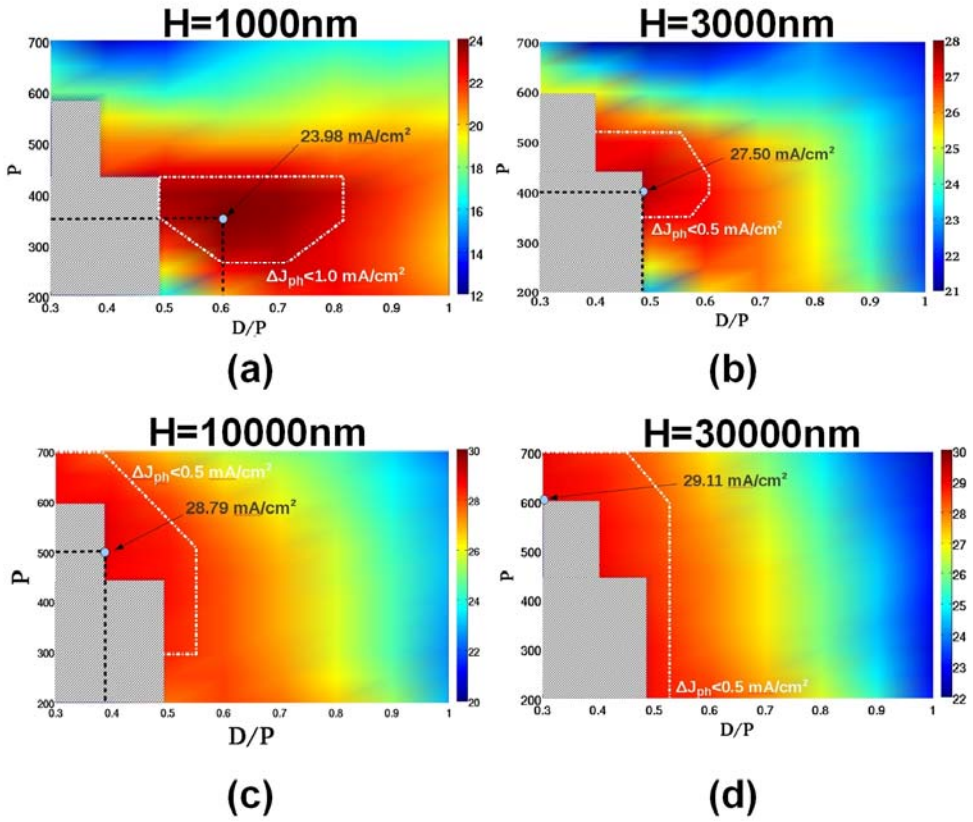

Figure 8 Photo-generated current density maps for the CdTe/ZnO/Glass nanowire array with height H=1000nm (a), 3000nm (b), 10μm (c) and 30μm (d). The optimum geometrical configurations (P=350nm-600nm, D/P=0.3-0.6) lead to J_{ph} within the range 23.98mA/cm^2-29.11mA/cm^2.

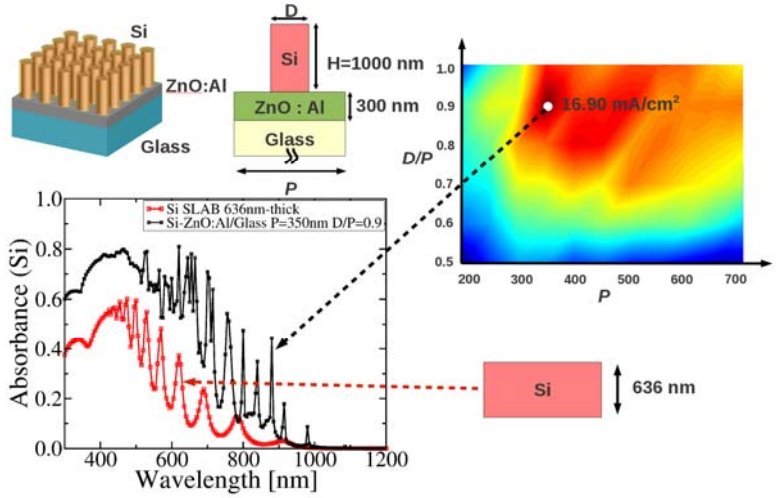

Figure 9 Comparison of the calculated absorbance characteristics of the optimized c-Si/AZO/Glass array (H=1000nm, P=350nm, D/P=0.9) and of the planar counterpart (silicon slab 636nm-thick); the enhancement in terms of photocurrent density J_{ph} is remarkable for the optimized nanowires based solar cell.

TCAD simulations (table 2) have shown that the performance of the nanowire is strongly affected by the bulk losses in a-Si (the doped shell layer, since in the interfacial layer the defect density is assumed to be significantly lower), by the recombination at the back electrode (the optical generation rate map shows that the carrier injection due to optical generation is relatively large at the back interface) and partially by the front electrode recombination. Probably the thickness of the doped a-Si shell should be reduced (to avoid the reduction of Jsc) and a p^+ a-Si thin layer (for instance 10nm-thick) should be placed between the c-Si core and the back electrode (AZO) like in case of heterojunction solar cells [6].

		IDEAL	A	B	C	D	E	F	G	H	I
Mobility (aSi)	cm2/Vs	100	0.10	0.10	0.10	0.10	0.10	100.00	100.00	100.00	0.10
Top electrode SRV	cm/s	1E+001	1.00E+007	1.00E+007	1.00E+001	1.00E+003	1.00E+007	1.00E+007	1.00E+007	1.00E+001	1.00E+001
Back electrode SRV	cm/s	1E+001	1.00E+007	1.00E+001	1.00E+007	1.00E+007	1.00E+003	1.00E+007	1.00E+001	1.00E+007	1.00E+001
c-Si LOSS		DIS	EN	EN	EN	EN	EN	DIS	DIS	DIS	DIS
a-Si LOSS		DIS	EN	EN	EN	EN	EN	DIS	DIS	DIS	EN
Jsc	mA/cm^2	17.95	9.17	9.29	9.17	9.17	9.29	14.38	14.49	17.83	9.29
Voc	V	0.772	0.438	0.740	0.438	0.438	0.635	0.449	0.766	0.455	0.753
FF		85.73	75.82	80.40	75.82	75.82	80.79	78.20	85.64	78.32	81.98
Eff	%	11.87	3.04	5.53	3.04	3.04	4.76	5.06	9.51	6.36	5.73

Table 2 : Simulation results. The symbol "DIS" means that bulk recombination mechanisms are disabled ; "ENS" means that, in case of a-Si, traps and radiative recombination are accounted for and, in case of c-Si, SRH trap-assisted, radiative and Auger recombination are accounted for.

3. Third activity : Optical and electrical characterisation of nanowires based solar cells

Confidential results restricted to the project until publication. Thank you for your understanding.

References

[1] Erik C. Garnett, Mark L. Brongersma, Yi Cui, and Michael D. McGehee, Nanowire Solar Cells, Annual Review of Material Research, 41:11.1–11.27, 2011.

[2] Michael D. Kelzenberg, ShannonW. Boettcher, Jan A. Petykiewicz, Daniel B. Turner-Evans, Morgan C. Putnam, Emily L.Warren, Joshua M. Spurgeon, Ryan M. Briggs, Nathan S. Lewis and Harry A. Atwater, "Enhanced absorption and carrier collection in Si wire arrays for photovoltaic applications", Nature Materials, Vol 9, March 2010.

[3] Fan, Z., Razavi, H., Do, J., Moriwaki, A., Ergen, O., Chueh, Y.-L., Leu, P. W., Ho, J. C., Takahashi, T.,Reichertz, L. A., Neale, S., Yu, K., Wu, M., Ager, J. W., and Javey, A., Three-dimensional nanopillar-array photovoltaics on low-cost and flexible substrates, Nat Mater 8, (2009) 648-653

[4] Tsakalakos, L., Balch, J., Fronheiser, J., Shih, M.-Y., LeBoeuf, S. F., Pietrzykowski, M., Codella, P. J.,Korevaar, B. A., Sulima, O. V., Rand, J., Davuluru, A., and Rapol, U., Strong broadband optical absorption in silicon nanowire films, Journal of Nanophotonics 1, (2007) 013552

[5] O'Donnell, B., Yu, L., Foldyna, M., and Roca i Cabarrocas, P., Silicon nanowire solar cells grown by PECVD, Journal of Non-Crystalline Solids , (2011)

[6] Takahiro Mishima, Mikio Taguchi, Hitoshi Sakata, Eiji Maruyama, Development status of high-efficiency HIT solar cells, Solar Energy Materials and Solar Cells, Volume 95, Issue 1, (2011, 18-21)

[7] Latu-Romain, E., Gilet, P., Feuillet, G., Noel, P., Garcia, J., Levy, F., and Chelnokov, A., Optical and electrical characterizations of vertically integrated ZnO nanowires, Microelectronics Journal 40, (2009) 224 -228

[8] Consonni, V., Rey, G., Bonaime, J., Karst, N., Doisneau, B., Roussel, H., Renet, S., and Bellet, D., Synthesis and physical properties of ZnO/CdTe core shell nanowires grown by low-cost deposition methods, Applied Physics Letters 98, (2011) 111906

[9] Schmidt-Mende, L., and MacManus-Driscoll, J. L., ZnO nanostructures, defects, and devices, Materials Today 10, (2007) 40 - 48

[10] Levy-Clement, C., Tena-Zaera, R., Ryan, M., Katty, A., and Hodes, G., CdSe-Sensitized p-CuSCN/Nanowire n-ZnO Heterojunctions, Advanced Materials 17, (2005) 1512-1515

[11] Wang, K., Chen, J. J., Zeng, Z. M., Tarr, J., Zhou, W. L., Zhang, Y., Yan, Y. F., Jiang, C. S., Pern, J., and Mascarenhas, A., Synthesis and photovoltaic effect of vertically aligned ZnO/ZnS core/shell nanowire arrays, Applied Physics Letters 96, (2010) 123105

[12] Zhang, Y., Wu, Z., Zheng, J., Lin, X., Zhan, H., Li, S., Kang, J., Bleuse, J., and Mariette, H., ZnO/ZnSe type II core/shell nanowire array solar cell, Solar Energy Materials and Solar Cells 102, (2012) 15 - 18

[13] Wang, X., Zhu, H., Xu, Y., Wang, H., Tao, Y., Hark, S., Xiao, X., and Li, Q., Aligned ZnO/CdTe Core/Shell Nanocable Arrays on Indium Tin Oxide: Synthesis and Photoelectrochemical Properties, ACS Nano 4, (2010) 3302-3308

[14] Putnam, M. C., Boettcher, S. W., Kelzenberg, M. D., Turner-Evans, D. B., Spurgeon, J. M., Warren, E. L.,Briggs, R. M., Lewis, N. S., and Atwater, H. A., Si microwire-array solar cells, Energy Environ. Sci. 3, (2010) 1037-1041

[15] J-M. Jin, *The Finite Element Method in Electromagnetics*. John Wiley & Sons, ISBN-10: 0471438189, 2002

[16] Whittaker, D. M. and Culshaw, I. S., Scattering-matrix treatment of patterned multilayer photonic structures.Vol. **60**, 4, pp. 2610-2618, 1999.

[17] K. S. Kunz and R. J. Luebbers. *The Finite Difference Time Domain Method for Electromagnetics*. CRC Press, 1993.

[18] M. G. Moharam and T. K. Gaylord. Rigorous coupled-wave analysis of planar grating diffraction. J. Opt. Soc. Am., **71** (7), pp. 811-818, 1981.

[19] M. Agrawal, M. Frei, Y. Bhatnagar, T. Repmann, K. Witting, J. Schroeder, and C. Eberspacher. Comprehensive experimental and numerical optimization of surface morphology of transparent conductive oxide films for tandem thin film photovoltaic cells. Proc. Of 35th IEEE Photovoltaic Specialists Conference (PVSC), 301-304, 2010.

[20] I. Semenikhin, M. Zanuccoli, M. Benzi, V. Vyurkov, E. Sangiorgi, C. Fiegna, Computational efficient RCWA method for simulation of thin film solar cells. Optical and Quantum Electronics, Vol. **44**, 3-5, 149-154, 2012

[21] P. Kailuweit, M. Peters, J. Leene, K. Mergenthaler, F. Dimroth, A.W. Bett, Numerical simulations of absorption properties of InP nanowires for solar cell applications. Prog. Photovolt: Res. Appl. doi: 10.1002/pip.1169, 2011

[22] Z. Pei, S-T. Chang, C-W. Liu, Y-C. Chen, Numerical Simulation on the Photovoltaic Behavior of an Amorphous-Silicon Nanowire-Array Solar Cell. Electron Device Letters, IEEE , vol. **30**, 12, pp.1305-1307, 2009

[23] *Sentaurus Device User Guide*, Version C-2009.06. Synopsys. Inc., 2009.

[24] C. Lin and M. Povinelli, Optical absorption enhancement in silicon nanowire arrays with a large lattice constant for photovoltaic applications. Opt. Express **17**, pp. 19371-19381, 2009.

[25] A.F. Oskooi, D. Roundy, M. Ibanescu, P.Bermel, J. D. Joannopoulos, and S.G. Johnson, MEEP: A flexible free-software package for electromagnetic simulations by the FDTD method. Computer Physics Communications **181**, pp. 687–702, 2010.

[26] L. Wen, Z. Zaho, X. Li, Y. Shen, H. Guo *et al*., Theoretical analysis and modeling of light trapping in high efficiency GaAs nanowire array solar cells. Appl. Phys. Lett. **99**, 143116, 2011

[27] M.D. Kelzenberg, M.C. Putnam, D.B. Turner-Evans, N.S. Lewis, H.A. Atwater, Predicted efficiency of Si wire array solar cells. Proc. Of 34th IEEE Photovoltaic Specialists Conference (PVSC), vol., no., pp. 001948-001953, 7-12 June 2009

[28] D. Bucci, B. Martin, and A. Morand, Study of propagation modes of bent waveguides and micro-ring resonators by means of the aperiodic Fourier modal method Physics and Simulation of Optoelectronic Devices XVIII, SPIE, 7597, 75970U, 2010.

[29] D. Bucci, B. Martin, and A. Morand. Application of the three-dimensional aperiodic Fourier modal method using arc elements in curvilinear coordinates J. Opt. Soc. Am. A, OSA, **29**, pp. 367-373, 2012.

[30] FDTD Solutions 7.5, Lumerical Solutions, Inc.

[31] ASTM G159-98 Standard Tables for References Solar Spectral Irradiance at Air Mass 1.5: Direct Normal and Hemispherical for a 37° Tilted Surface (Withdrawn 2005), DOI: 10.1520/G0159-98

[32] S.W. Glunz, S. Rein, J.Y. Lee, W. Warta, Minority carrier lifetime degradation in boron-doped Czochralski silicon. Journal of Applied Physics, Vol. **90**, 5, pp. 2397-2404, 2001.

[33] A. Schenk, "Finite-temperature full random-phase approximation model of band gap narrowing for silicon device simulation", Journal of Applied Physics, Vol. **84**, 7, pp. 3684-3695, 1998.

[34] P.P. Altermatt, Models for numerical device simulations of crystalline silicon solar cells – a review. J. Comput. Electron., Vol. **10**, 3, pp. 314-330, 2011.

[35] D.B.M. Klaassen, A unified mobility model for device simulation: I. model equations and concentration dependence. Solid-State Electronics, Vol. **35**, 7, pp. 953-959, 1992.

[36] J. Kumar, S.K. Manhas, D. Singh, R. Vaddi, Optimization of vertical silicon nanowire based solar cell using 3D TCAD simulation. 13th International Symposium on Integrated Circuits (ISIC), pp.528-531, 12-14 Dec. 2011

[37] Hu, L., and Chen, G., Analysis of Optical Absorption in Silicon Nanowire Arrays for Photovoltaic Applications, Nano Letters 7, (2007) 3249-3252

[38] Li, J., Yu, H., Wong, S. M., Zhang, G., Sun, X., Lo, P. G.-Q., and Kwong, D.-L., Si nanopillar array optimization on Si thin films for solar energy harvesting, Applied Physics Letters 95, (2009) 033102

[39] Li, J., Yu, H., Wong, S. M., Li, X., Zhang, G., Lo, P. G.-Q., and Kwong, D.-L., Design guidelines of periodic Si nanowire arrays for solar cell application, Applied Physics Letters 95, (2009) 243113

[40] Alaeian, H., Atre, A. C., and Dionne, J. A., Optimized light absorption in Si wire array solar cells, Journal of Optics 14, (2012) 024006

[41] Huang, N., Lin, C., and Povinelli, M. L., Broadband absorption of semiconductor nanowire arrays for photovoltaic applications, Journal of Optics 14, (2012) 024004.

[42] AllenJE, Hemesath ER, Perea DE, Lensch-Falk JL, Li ZY, High resolution detection of Au catalyst atoms in Si nanowires, Nature Nanotechnology 3 (3) (2008) 168-173.

[43] Kelzenberg MD, Turner-Evans DB, Kayes BM, Filler MA, Putman MC, Photovoltaic measurements in single nanowire silicon solar cells, Nano Lettes 8 (2) (2008) 710-714.

[44] Bryce B., Reuter M., Wacaser B., Tiwari S. , Contactless measurement of surface dominated recombination in gold and aluminum catalyzed silicon vapor liquid solid wires, Nano Letters, 11 (2011) 4282-4287.

[45] Jung Y., Vacic A., Perea D., Picraux S. , Reed M., Minority carrier lifetime and surface effects in VLS-Grown axial p-n junction silicon nanowires, Advanced Materials 23 (2011) 4306-4311.

[46] Coutaz J.L., Optoélectronique Terahertz, EDP Sciences, France , 2008, 360 pages.

[47] Brendan M. Kayes, Harry A. Atwater, Comparison of the device physics principles of planar and radial nanorod solar cells, Journal of Applied Physics 97, 114302 (2005).